An Endorectal Ultrasound Probe Comanipulator With Hybrid Actuation Combining Brakes and Motors

Cécile Poquet, Pierre Mozer, Marie-Aude Vitrani, and Guillaume Morel

***Abstract*—A robotic device, aimed at assisting a urologist in positioning an endorectal ultrasound probe to perform prostate biopsies, is presented. The proposed system is a comanipulator that holds the probe simultaneously with the urologist. This robot supports two modes of operation: the free mode, where the entire movement control is left to the urologist when he/she positions the probe with respect to the prostate thanks to the feedback provided by the ultrasound images; the locked mode, where the robot's role is to precisely maintain the targeted biopsy site at a given location, while the urologist can insert a needle through a guide mounted on the probe and proceed to biopsy. The device combines three brakes and three motors. This allows both transparent comanipulation in the free mode with six degrees of freedom liberated and stabilization of the probe in the locked mode. At the control level, a main challenge in the locked mode raises from antagonistic constraints: the needle placement shall be precise in spite of unknown external forces due to the contact between the probe and the rectum; the robot apparent impedance shall be low due to security constraints. This is solved by an inner low stiffness controller and an outer slow integration for canceling steady-state errors. Both *in vitro* and *in cadavero* experimental results show the efficiency of the system in the two modes of operation.**

***Index Terms*—Medical robotics, robot control.**

I. Introduction

In 2013, more than 230 000 new prostate cancer cases have been detected in the USA, thanks to the hundreds of thousands of biopsy procedures [1]. Prostate biopsy is indeed the medical examination used to diagnose a prostate cancer. It consists of sampling the prostate tissue using a biopsy needle.

An examination includes 12 samples equally distributed across the prostate volume. A major technical difficulty arises from the desired precision for the needle placement, which typically reaches a few millimeters [2], [3]. Achieving such a precision is difficult because the prostate has a variable volume, experiences large displacements (up to 1 cm), and significantly deforms [4], [5]. Meanwhile, obtaining a high precision and control of the 3-D needle placement constitutes a major medical issue for the prostate biopsy procedure. Indeed, it may lead to obtaining a fine 3-D map of cancerous regions in the prostate which is required for allowing the development of local therapy instead of total prostate ablation, which is the most common treatment of prostate cancer today. Prostatectomy induces a high rate of side effects, such as incontinence and is more and more considered as an unnecessary surgery for a number of patients, accounting for the very slow development of certain cancers. The broad development of local therapy (namely by creating a necrose in a small region of the prostate) will be possible only when the biopsy procedure precision will have significantly increased as compared to current practice. Note also that placing a needle in a prostate with high precision is required for brachytherapy, which consists of inserting radioactive seeds through a needle across the prostate volume in order to irradiate the cancerous tissue.

Because of its crucial importance in terms of public health, robotic assistance to needle placement in the prostate has been the object of interest for the robotics community in the past years. A recent exhaustive overview of these systems can be found in [6].

Imagery is a first feature that can be used to classify the systems proposed across the literature. Since the prostate deforms and moves during a needle placement procedure, it is required to monitor the needle placement using intraoperative imaging. Throughout the literature, authors propose to use ultrasound imaging (USI) [6]–[8], MRI [9]–[11], or CT Scan [12]. USI provides either 2-D planar images in real time or 3-D images at a few seconds rate. Two-dimensional USI is often coupled with a stepper: thanks to successive incremental penetration movements of the probe, a series of parallel cross-sections are acquired and assembled to provide a 3-D image [7], [8], [13]–[16]. USI is largely available in urologist consulting rooms at a reasonable cost. MRI or CT scan imaging provide better images at a higher cost and lower frequency. MRI also imposes drastic constraints on the design of the robot due to magnetic compatibility [9], [11] and CT scan brings problems due to irradiation doses for both the urologist and the patient. In order to be compatible with the medico–economic constraints of the biopsy procedure and in accordance with the most common practice across urologists worldwide, our system, called Apollo, exploits an endorectal ultrasound imaging.

Manuscript received August 5, 2013; revised December 11, 2013; accepted February 14, 2014. Date of publication April 21, 2014; date of current version October 3, 2014. Recommended by Technical Editor E. Richer. This work was supported by French state funds managed by the ANR within the Invesissements d'Avenir Program (Labex CAMI) under Reference ANR-11-LABX-0004 and through the PORSBOT Project under Reference ANR-11-TECS-0017. This work was presented in part at the IEEE/RSJ International Conference on Intelligent Robots and Systems, Tokyo, Japan, November 3–8, 2013.

C. Poquet, M.-A. Vitrani, and G. Morel are with the Sorbonne Universités, UPMC University Paris 06, UMR 7222, ISIR, F-75005 Paris, France, and CNRS, UMR 7222, ISIR, F-75005 Paris, France, and also with the INSERM, U1150, Agathe-ISIR, F-75005 Paris, France (e-mail: poquet@isir.upmc.fr; marie-aude.vitrani@upmc.fr; guillaume.morel@upmc.fr).

P. Mozer is with the Sorbonne Universités, UPMC University Paris 06, UMR 7222, ISIR, F-75005, Paris, France, and CNRS, UMR 7222, ISIR, F-75005 Paris, France and with the INSERM, U1150, Agathe-ISIR, F-75005 Paris, France, and also with the AP-HP, Hôpital de la Pitié Salpêtrière, Service d'Urologie, F-75013 Paris, France (e-mail: mozer@isir.upmc.fr).

Color versions of one or more of the figures in this paper are available online at http://ieeexplore.ieee.org.

Digital Object Identifier 10.1109/TMECH.2014.2314859

Robotic systems found in the literature can also be classified by the needle access: needles can be placed in the prostate either through transperineal access, [6], [12]–[18], or through transrectal access, [19], [20]. In the clinical conventional practice, for a biopsy procedure, a transrectal access is exclusively adopted. The patient is placed in a lateral decubitus or lithotomy position and a local anesthesia of the rectal region is performed. He is awake, and thus, he may move during the procedure. Endorectal needle placement is usually associated with endorectal ultrasound imaging: the needle guide is attached to the USI probe and both are inserted simultaneously in the rectum. As a result, the needle position is known in the probe image frame. Prior to its insertion, it can be visualized by a straight line on the screen displaying the image. Transperineal needle placement is generally used for brachytherapy, with a patient placed in the lithotomy position. Some authors also suggest to use transperineal access for biopsies [11], but the procedure is slower and requires total anesthesia, which does not seem compatible with the medico–economic constraints. Apollo exploits a transrectal access for the needle, through a guide attached to the USI probe, because it is compatible with the current practice and simplifies the robot design without adding constraints due to imagery.

The robot kinematics is the third factor distinguishing the existing robots that assist the placement of a needle in the prostate. The number of degrees of freedom (DoF) required to place the tip of a needle at an arbitrary position with an arbitrary needle axis orientation is 5 and not 6, since the rotation of the needle around its penetration axis does not affect the tip position nor the axis orientation. Some authors use six active DoF, the actuation of the rotation around the needle axis being used to improve the needle penetration through the perineum, [6]. For robots manipulating an endorectal USI probe, like Apollo, the anus plays the role of a 2-DoF kinematic constraint. Only 4-DoF are to be used: three rotations around the penetration point and one translation along the penetration axis. This has led to the design of robots exhibiting a remote center of motion [14]. A clear benefit of this approach is that only four actuated DoF are required, which participates to reducing the cost. A major drawback is that, prior to operation, a setup phase is required to place the remote center of motion, which is fixed with respect to the robot base, and must coincide with the patient's anus. Moreover, in a study where the endorectal USI probe displacements during clinical practice have been monitored, it has been observed that the anatomical constraint is not perfectly respected during manual operation [21]. Due to other geometrical constraints (from anatomy and from needle guide placement that should leave an easy access to the urologist), it seems to be useful to produce small movements that do not strictly leave the entry point at a fixed position. For these reasons, Apollo possesses six DoF in such a way that its placement with respect to the patient's anatomy is not imposed, and the urologist can slightly displace the anus when required for an optimal probe placement.

Finally, the last criteria for classifying the literature is the degree of automation. Some devices are fully automated: the robot is registered with respect to the prostate, the needle desired localization is given by a preoperative planning and the robot autonomously places the needle [15]. This is of particular interest for devices guided by CT scan images, since the urologist can stand far away from the CT scanner, reducing the exposure to irradiations. Some devices are comanipulators, in the sense that the gesture control is shared by the robot and the urologist. The most frequent scenario for this approach involves the robot placing the needle guide and the needle itself being placed by the urologist [8], [14], [19].

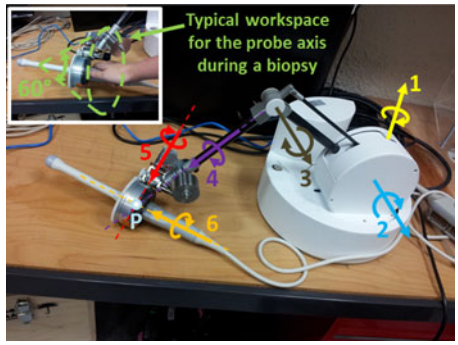

Fig. 1. General view of the proposed probe comanipulator.

Apollo, which is described in more detail in Section II, fits in the category of comanipulators, although it differs from the existing systems by the functions is provides. Instead of separating between robotic autonomous probe placement and human needle placement, it lets the urologist positioning the probe. This choice is motivated by the difficulty of planning a trajectory for the probe positioning when accounting for prostate deformations and displacements, eventual movements from the patient, anus, and rectum anatomical constraints, etc. Apollo is thus offering a *free mode*, where it leaves the probe motion as free as possible (see Section III). This allows for manually positioning the probe under USI guidance. Then, Apollo provides a second function: the *locked mode*, during which the urologist has his/her hands free to perform the needle placement and the biopsy. Here, it is desired that the robot maintains precisely the target position, while preserving the patient's safety. This is antagonistic in the context of robot control: usually precision is achieved thanks to a high stiffness while safety, for a robot in contact with a human, requires a low impedance. The locked mode is presented, together with *in-vitro* experiments, in Section IV. Two cadaver experiments are also reported in Section V, confirming the performances observed during *in-vitro* experiments.

II. Proposed System

A. Apollo's Kinematics

A picture of Apollo is given in Fig. 1. As justified in Section I, it exhibits 6-DOF to be compatible with all the required probe movements while avoiding to constrain its placement with respect to the patient. While the robot base is placed at an approximate distance of 40 cm from the entry point, on the examination table, it allows the probe to cover the required workspace. This workspace was determined from clinical data recorded during 78 prostate biopsy procedures, see [21]. It can be modeled by a cone, whose origin coincides with the anatomical entry point, and whose angle is typically 60° (see Fig. 1, upper left corner).

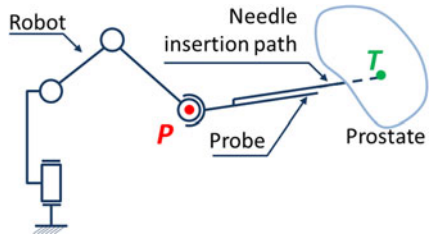

Fig. 2. Apollo's kinematics.

TABLE I
DENAVIT AND HARTENBERG PARAMETERS OF THE COMANIPULATOR

i	α_{i-1}	a_{i-1}	d_i	θ_i
1	0	0	0	θ_1
2	$-\pi/2$	0	0	θ_2
3	0	0.25 m	0	θ_3
4	$\pi/2$	0	0.3 m	θ_4
5	$-\pi/4$	0	0	θ_5
6	$\pi/2$	0	0	θ_6

Apollo is made of six pivot joints serially assembled according to a conventional anthropomorphic geometry: the three first joints form the shoulder and the elbow while the wrist is composed of the three last joints, whose axes coincide at Point P (see Fig. 1). The kinametics is sketched in Fig. 2, where Point P is the wrist center while Point T is the biopsy target location, whose location is known in the robot end-effector frame. Note that Point P position with respect to the robot base only depends on the three first joint positions, which are measured thanks to encoders, while Point T position also depends on the wrist joint positions, which are measured thanks to high resolution potentiometers. Kinematic models mapping joint positions into Point P or Point T positions follows directly from the Denavit and Hartenberg parameters given in Table I, [22].

The last pivot axis is designed in such a way that it leaves a 8-cm diameter cylindrical hole whose axis coincides with the rotational axis. Therefore, an interface part can be designed to adapt to any specific probe shape and to connect to the robot end-effector in such a way that the probe insertion axis coincides with the robot's joint six axis. This part is fixed on the probe and can be placed into the robot end effector thanks to a mechanical connector involving magnets (see Fig. 3).

B. Actuation

In order to obtain the locked mode, the system must be actuated. Since there is no need for active motion, a first guess solution is to mount brakes on all the six robot's joints. However, this would require an infinite stiffness for both the brakes and the robot structure. Indeed, once the urologist has positioned the probe at a desired location and sets up the locked mode, he/she releases the probe handle to manipulate the needle and the biopsied tissues. Then, all the external forces that the urologist was compensating for in the free mode, namely the probe weight and the interaction wrench applied to the patient through the probe, act as disturbances for the robot when he/she releases the probe. If the robot's stiffness with the brakes on is not infinite, this will lead to a displacement of the targeted site.

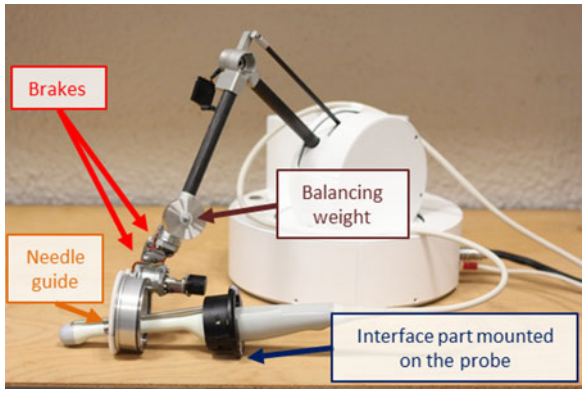

Fig. 3. View of the interface part used to mount the probe. It allows a 340° rotation of the probe around its axis. A hole is left to insert the biopsy needle guide.

Achieving a very high stiffness for both the robot structure and the brakes can be done only by increasing the robot weight and the brakes power. Altogether, this would be detrimental to the robot's lightness (or *transparency*), which is crucial for the free mode.

In order to maintain a high transparency (low friction, low weight, and low inertia) for the robot's free mode, while being able to keep the biopsy target at a precise location despite unknown disturbances in the locked mode, a hybrid actuation system is chosen.

1) For the three wrist joints, small electromagnetic brakes are installed (Kebco 01.P1.300). The control of the brakes is binary: the brakes are either blocked (ON), which corresponds to the unpowered state, or free (OFF), which corresponds to powered state. Therefore, in case of a loss of power, the wrist will be freezed to its configuration. Brakes provide a null torque when they are OFF. When they are ON, they exhibit a high resistive torque with a low mass.
2) To be able to compensate for the possible displacements due to external forces, electric motors (Maxon RE35) are mounted on the three first joints. In order to maintain a high transparency in the free mode,the following are employed.
   a) The motors are placed near the robot base, in such a way that their mass does not significantly affect the robot's inertia.
   b) A cable transmission is used to limit joint friction.
   c) Load springs are mounted on joints 2 and 3 to compensate for the robot weight.

In the low-level electronics, a current loop allows controlling the motor torque. The control input for the three first joints' motors is the current i_i, $i \in \{1 \cdots 3\}$, which corresponds to a joint torque τ_i up to a scalar factor k_{τ_i} accounting for the motor torque constant and the transmission ratio

$$\tau_i = k_{\tau_i} i_i, \quad i \in \{1 \cdots 3\}. \tag{1}$$

In the following, the torque is considered as the control input for the three first joints' motors, knowing that the corresponding input current can be computed thanks to (1).

TABLE II
ACTUATION DATA

Joint	Actuator	Transmission	Ratio	Max. torque
1	motor	cable	21.6	3.4 Nm
2	motor	cable	14.9	2.4 Nm
3	motor	cable	14.8	2.3 Nm
4	brake	direct	1	0.4 Nm
5	brake	direct	1	0.4 Nm
6	brake	gear	4.5	1.8 Nm

The robot was manufactured by the French company Haption, [23], and exploits the Haption technology dedicated to high forces haptic interfaces for the three first joints. All the characteristics of the actuation system are summarized in Table II.

III. FREE MODE

A. Control

The computation of the torques for the free mode is primarily based on the kinematic model

$$\begin{pmatrix} \mathbf{v}_{6/0}(P) \\ \omega_{6/0} \end{pmatrix} = \underbrace{\begin{pmatrix} \mathbf{J}_{v1,P} & \mathbf{0} \\ \mathbf{J}_{\omega 1} & \mathbf{J}_{\omega 2} \end{pmatrix}}_{\mathbf{J}_P} \dot{\mathbf{q}} \tag{2}$$

where $\mathbf{v}_{a/b}(N)$ stands for the velocity of a point N produced in the motion of frame $\mathscr{F}_a$ with respect to frame $\mathscr{F}_b$, $\omega_{a/b}$ stands for the rotational velocity of frame $\mathscr{F}_a$ with respect to frame $\mathscr{F}_b$, $\dot{\mathbf{q}} = [\,\dot\theta_1 \;\cdots\; \dot\theta_6\,]^{\mathrm{T}}$ is the joint velocity vector, $\mathbf{J}_P$ is the 6×6 robot jacobian matrix at Point P and $\mathbf{J}_{v1,P}$, $\mathbf{J}_{\omega 1}$ and $\mathbf{J}_{\omega 2}$ are 3×3 jacobian submatrices. Note that the upper right null submatrix indicates that the three last joint movements do not affect the velocity of Point P, which is the points where the wrist axes intersect.

In the rest of the paper, we will assume full rank for $\mathbf{J}_P$ (and thus for $\mathbf{J}_{v1,P}$, $\mathbf{J}_{\omega 1}$ and $\mathbf{J}_{\omega 2}$), which is practically guaranteed in the prototype due to joint physical limits that leave kinematic singularities out of the workspace.

Due to kinemato-static duality, the transpose of the Jacobian matrix defined in (2) can be used to map an external wrench applied to the environment through the end-effector into the vector of joint torques $\tau = [\,\tau_1 \;\cdots\; \tau_6\,]^T$:

$$\tau = \begin{pmatrix} [\tau_1 \;\; \tau_2 \;\; \tau_3]^T \\ [\tau_4 \;\; \tau_5 \;\; \tau_6]^T \end{pmatrix} = \underbrace{\begin{pmatrix} \mathbf{J}_{v1,P}^T & \mathbf{J}_{\omega 1}^T \\ \mathbf{0} & \mathbf{J}_{\omega 2}^T \end{pmatrix}}_{\mathbf{J}_P^T} \begin{pmatrix} \mathbf{f}_{6\to\mathrm{ext}} \\ \mathbf{6}_{\to\mathrm{ext}}(P) \end{pmatrix} \tag{3}$$

where $\mathbf{f}_{6\to\mathrm{ext}}$ is the force applied by the robot end-effector on the environment and $\mathbf{m}_{6\to\mathrm{ext}}(P)$ is the moment applied by the robot end-effector on the environment at Point P. In the free mode, the brakes being OFF, the joint torques τ_4 to τ_6 are null. Therefore, from the second line of Eq. (3), it can be seen that the exerted wrench has a null moment at Point P: $\mathbf{m}_{6\to\mathrm{ext}}(P) = \mathbf{0}$. In other words, Eq. (3) simplifies to

$$(\,\tau_1 \quad \tau_2 \quad \tau_3\,)^T = \mathbf{J}_{v1,P}^T \mathbf{f}_{6\to\mathrm{ext}}. \tag{4}$$

The robot links weight is balanced by counterweights and springs in such a way that there is no need for compensation of the robot weight by the actuators. Compensating for the probes weight is desirable in both modes:

1) in the free mode, it will ease the comanipulation as the user would not have to carry the probe weight.
2) in the locked mode, gravity compensation will limit the effect of the total external disturbance, which consists of the sum of the weight (known, then compensable) and the probe-rectum interaction force (a priori unknown).

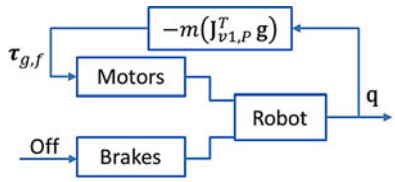

Fig. 4. FMC scheme.

The external wrench applied to the probe and its interface at Point P, due to gravity is

$$\begin{pmatrix} \mathbf{f}_{g\to 6} \\ \mathbf{m}_{g\to 6}(P) \end{pmatrix} = \begin{pmatrix} m\mathbf{g} \\ m\mathbf{d}_{PG} \times \mathbf{g} \end{pmatrix} \tag{5}$$

where m and G are the mass and the center of gravity of the probe and its interface, respectively, $\mathbf{g}$ is the gravitational field vector, and $\mathbf{d}_{PG}$ is the vector from P to G. Balancing experiments lead to identify $m = 0.5$ kg and $\mathbf{d}_{PG} = -d\mathbf{z}_6$, where $d = 9$ mm and $\mathbf{z}_6$ is the unit vector parallel to the probe penetration axis, directed towards the prostate.

Compensating for gravity in the free mode straightforwardly derives from (4) and (5)

$$\tau_{g,f} = (\,\tau_1 \quad \tau_2 \quad \tau_3\,)^T = -m\mathbf{J}_{v1,P}^T \mathbf{g}. \tag{6}$$

This controller is referred in the next as free mode control (FMC) and is depicted in Fig. 4.

B. Experimental Evaluation

In the free mode, Apollo's design and control are aimed at minimizing forces applied to the US probe, in such a way that the urologist does not feel any resistance when moving the probe. This property, namely the ability of a comanipulated robot to not resist to any users motor intention, is called transparency. A perfectly transparent robot would apply an exactly null force to the probe, whatever the motion imposed to the probe by the urologist. Of course, this is impossible, due to even small joint friction, links and motors inertia, and robot bandwidth limitation. As a consequence, from the user side, moving the probe may become uneasy in the free mode. The movements can be altered as compared to natural movements [24] and this may result in a lack of manipulability when pointing a biopsy target site. Therefore, it is important to evaluate Apollo's transparency in order to ensure that, during practical practice, the manipulation of the probe by the urologist to place the needle guide will not be disturbed.

In order to evaluate Apollo's transparency, it is thus required to perform probe positioning tasks with and without the robot connected to the probe and to compare the motion characteristics. To this aim, an *in-vitro* experiment has been set up. It

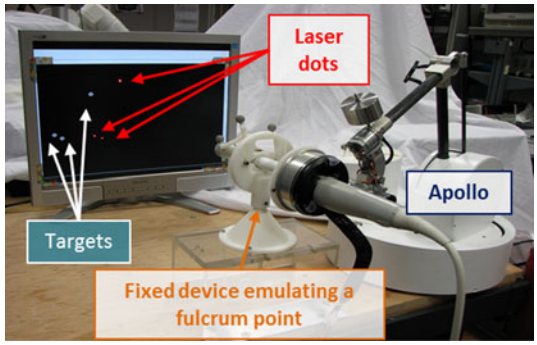

Fig. 5. Experimental setup used to evaluate Apollo's transparency.

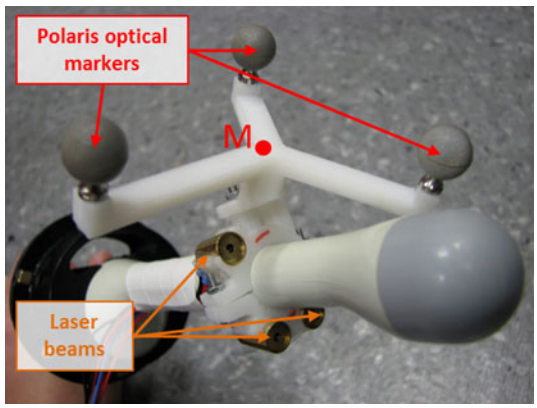

Fig. 6. Distal part of the probe equipped with laser beams and a Polaris target.

reproduces the geometry of a real examination: the movements that the subjects have to realize with the probe are similar to those of an urologist performing prostate biopsies. They require a control of the four DoF (three orientations + one penetration along the probe axis).

Each subject has to perform repeated pointing tasks with the probe passing through a fixed orifice figuring a patients anus (see Fig. 5). One, thus, can compare how subjects execute a sequence of several movements of the probe under visual guidance when the probe is either connected to Apollo under FMC or not connected to any device.

The probe distal part has been equipped with three laser pointers which beams diverge and do not feature any geometrical particularity (no parallelism, nor intersection) as illustrated on Fig. 6. When the beams are on, they project three dots on a fixed screen. As the probe passes through a hole which is attached to the table, one unique position and orientation of the probe corresponds to a given position for the three laser dots on the screen.

The subjects have been asked to perform pointing tasks. They were presented with an image made of three white dots on a black background (see Fig. 5). Once they had managed to place each of the laser dots in its target, another image (thus, another set of targets) was displayed. A set of six images has been used repeatedly.

In order to avoid any learning effect, the subjects were asked to perform the pointing task endlessly. Once the time needed to perform the task for one set of six images was stable, the initial

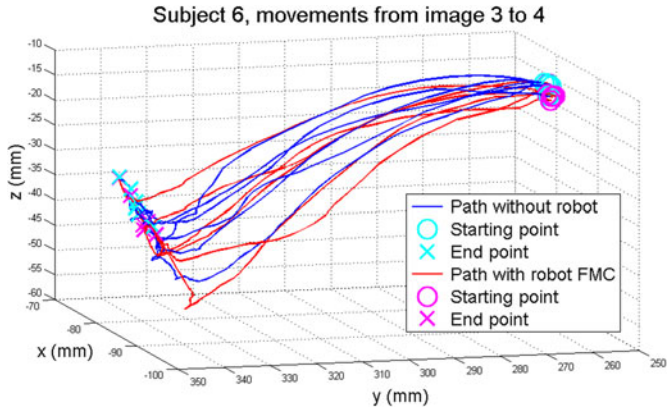

Fig. 7. Trajectories of point M recorded between Images 3 and 4 for Subject 6, with and without Apollo connected to the probe.

learning phase was considered to have reached its end and the experiment itself began.

The subjects had to perform the pointing task six times on the set six of images under each of the following conditions:

1) without Apollo: holding the probe with their hand, the probe not being mounted on the robot.
2) with Apollo: holding the probe with their hand, the probe being mounted on the robot under FMC.

These two conditions were presented to each subjects in a random order. Twelve nave subjects have been involved in this experiment, all of them male, aged 21 to 30, without experience in prostate needle placement.

To measure the probe position independently from the presence of the robot, a stereoscopic localization system was used (Polaris, NDI, Canada). Two Polaris optical targets were designed: one is fixed to the probe distal part (see Fig. 6), the other is attached to the robot base as a reference. This allows to measure and record the position $\mathbf{x}_M$ of a point M attached to the optical target mounted on the probe with respect to the frame defined by the optical target mounted on the robot base.

C. Results

As a typical example, Fig. 7 shows the trajectories recorded for Point M when a given subject was moving from the position where the three laser dots match the three targets of Image 3 to reach the position where the three laser dots match the three targets of Image 4. It can be observed that the trajectories are similar, exhibiting a first phase where the subject essentially adjusts the orientation (and thus, Point M essentially describes an arc) and a second phase where the depth is mainly controlled (and thus, Point M mostly follows a straight line). This seems to indicate a lack of influence of the presence of Apollo in the movements.

In order to quantitatively compare the subjects' performance during the positioning task under the two conditions, two indicators were selected:

1) the task duration t_d, which is the time it takes for a given subject under a given condition to place the laser dots on each of the six images constituting an image set.

TABLE III
SUMMARY OF THE DATA EXTRACTED DURING POINTING TASKS

	Average time by image set (in s)		Average SAL by image set	
	Without Apollo	With Apollo in FMC	Without Apollo	With Apollo in FMC
Subject 1	16.2	27.5	-9.96	-11.54
Subject 2	19.4	23.3	-10.02	-11.08
Subject 3	26.0	24.0	-12.60	-13.94
Subject 4	22.6	19.8	-10.96	-9.28
Subject 5	30.9	29.6	-13.53	-11.85
Subject 6	25.8	26.9	-9.63	-9.62
Subject 7	25.4	25.9	-12.97	-11.07
Subject 8	24.2	25.7	-14.42	-12.77
Subject 9	17.1	21.0	-9.37	-8.11
Subject 10	21.5	21.4	-10.97	-10.88
Subject 11	25.2	25.7	-9.80	-9.80
Subject 12	27.5	29.6	-12.42	-11.53
Average	23.5	25.0	-11.39	-10.96

2) the spectral arc length (SAL) of the trajectories for Point M as defined in [25]; SAL is the opposite of the length along the spectral curve of a movement; not only it is an image of the complexity of the movement Fourier magnitude spectrum, but it is also dimensionless and independent of the movement magnitude and duration; its value is negative; the closer it is from zero, the simpler the movement Fourier spectrum is and, thus, the smoother the movement is.

Note that the precision of the task by itself is imposed since a new image is presented to the subject only when he/she has properly positioned each if the three laser spots on each of the three screen targets for a given image. Therefore, the task duration is an indirect measurement for the precision as well.

Table III presents the task duration t_d and the SAL, averaged across the six trials, for each subject and condition. Comparing the mean values (and variances) of these two indicators for each condition does not allow drawing any conclusion by itself. It needs to be completed by, e.g., a student t-test. This is a statistical test that evaluates whether a difference experimentally observed between two groups of measured values (with a little number of measures) is statistically significant or not. Two student t-tests were performed on the full set of data (six measures by subject and by condition, thus two groups of 72 values for each test) to assess the effect of Apollo on the task completion time and on the movements smoothness during a pointing task. The p-values are, respectively, 0.0690 and 0.0796. Note that in general, in the literature of human motion analysis, a difference between observed mean values is said to be statistically significant when the p-value is smaller than 0.05.

D. Discussion

Table III shows that the measured average indicators are almost the same for the two conditions, leading to the conclusion that Apollo is appropriately transparent. More precisely:

1) The task completion time is, in average, 1.5 s higher with the robot than without; this is negligible in the clinical context as a prostate biopsy examination typically lasts 20 to 30 min.
2) In average, the SAL differs only by 0.43 between the two conditions. The movement is slightly smoother when Apollo is holding the probe and performing gravity compensation, but the indicator means are very close in the two conditions.

A statistical analysis of significance through the student t-test shows that for the two indicators, p-values are larger than 0.05. This can be interpreted in two ways: either there is really a difference between the mean indicator values, according to the measured average in Table III, but this difference is so small as compared to the indicator variances that it can be finely estimated only through a larger number of experiments; or there is no difference, which again would require more experiments to be statistically proven.

In any cases, the series of experiments conducted with 12 subjects allows to conclude that in practice, Apollo configured in the free mode does not affect the gesture smoothness or duration in such a way that it could impact the clinical practice. In other words, Apollo is transparent enough in the free mode for the targeted application.

TABLE IV
THE THREE CONTROLLERS PROPOSED FOR THE LOCKED MODE DIFFER IN THE EQUIPMENT THEY REQUIRE FOR THE WRIST JOINTS

Controller	Wrist brakes	Wrist Position Sensors
LMC-A	No	No
LMC-B	Yes	No
LMC-C	Yes	Yes

IV. LOCKED MODE

A. Control

For the locked mode, we propose three different controllers, labeled LMC-A to LMC-C (Locked Mode Control, A to C). Our aim is to evaluate whether the use of active brakes and/or position measurement is required for the wrist joints. This has a crucial importance in the future development of a clinical application, where the cost and complexity of the device are key issues. Table IV summarizes the main differences between the three controllers. Namely, the brakes are not used for controller LMC-A, while only controller LMC-C is exploiting the wrist joint position sensor.

1) First Controller: The first controller, hereinafter LMC-A, does not use the brakes or the wrist joint position sensors. Our idea here is to use only the three motors to guarantee that, once the robot is switched to the locked mode, the position of Point P is maintained constant. In this case, because of the friction between the probe and the rectum, it may be possible to obtain a constant position and orientation. This will depend on the magnitude of the elastic forces between the probe and the patient, that may influence the probe orientation around Point P.

For this controller, the gravity compensation is the same as for the free mode, while a torque is added to emulate an elastic

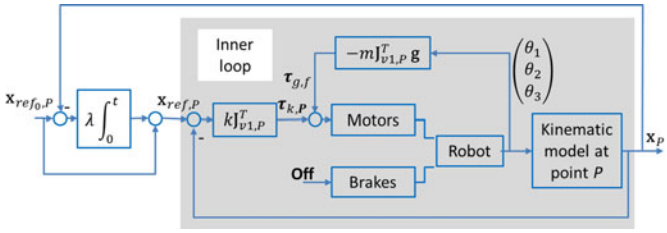

Fig. 8. First control scheme in the locked mode (LMC-A).

behavior at Point P

$$\tau_{\mathrm{LMC-A}} = \tau_{g,f} + \tau_{k,P} \tag{7}$$

where

$$\tau_{k,P} = \mathbf{J}^T_{v1,P} k(\mathbf{x}_{\mathrm{ref},P} - \mathbf{x}_P). \tag{8}$$

In this last equation, k is a stiffness coefficient, $\mathbf{x}_P$ is the position of Point P in the fixed frame $\mathscr{F}_0$, which can straightforwardly be computed from the three first joint positions through the robot's direct kinematics model, and $\mathbf{x}_{\mathrm{ref},P}$ is the position of Point P recorded when the urologist activates the locked mode from the free mode. In other words, it is the position where Point P shall stay still.

It is desirable to tune a low stiffness for security reasons. Indeed, during a biopsy procedure, the patient may be moving and the resulting forces should not be too large. In practice, a stiffness as low as $k = 200$ N/m is selected. As a result, it was experimentally found that the residual joint friction of the device, although rather low, was enough to damp out the oscillations without using a velocity feedback. However, in this case, the efforts applied to the rectum and the prostate may induce significant displacements for Point P. To compensate for this, an outer integral compensation is added. The reference position is changed with a rate

$$\dot{\mathbf{x}}_{\mathrm{ref},P} = \lambda\left(\mathbf{x}_{\mathrm{ref}_0,P} - \mathbf{x}_P\right) \tag{9}$$

where λ is a scalar gain in s^{-1} and $\mathbf{x}_{\mathrm{ref}_0,P} = \mathbf{x}_{\mathrm{ref},P}$ when the urologist sets the locked mode on. In other words,

$$\mathbf{x}_{\mathrm{ref},P} = \mathbf{x}_{\mathrm{ref}_0,P} + \lambda \int_0^t \left(\mathbf{x}_{\mathrm{ref}_0,P} - \mathbf{x}_P(u)\right) du. \tag{10}$$

Thanks to this integrator, when the urologist releases the probe after setting on the locked mode, the probe initially moves due to the wrench applied to the patient, but the resulting positioning error is then compensated for thanks to a modification of the reference position.

Combining Eq. (10) with Eq. (7) and Eq. (8), one finally gets a controller in the locked mode that could be written as an equivalent conventional PI compensator for the position error (see Fig. 8). What is particular here is the external loop implementation for the integrator and the associated tuning method: a low stiffness k is first chosen (200 N/m); then, the external integral gain λ is chosen to adjust the time required to compensate for a disturbance. It is not required to select a high value for λ. A slow compensation will ensure a correction of the position within a few seconds, which is acceptable for the clinical application. It will not significantly change the stiffness at the frequencies that are typical for a human-robot interaction (from 0.5 to 3 Hz). Furthermore, for safety reasons, the integration can be stopped either when the error will have become null, after a few seconds, or when the force applied by the controller exceeds a tunable limit. In practice, the external integrator was tuned thanks to experiments in which an error of 1 cm induced by an external load should be corrected in approximately 5 s thanks to integration. This lead to $\lambda = 4\ \mathrm{s}^{-1}$.

2) Second Controller: Because maintaining constant the position of Point P while the wrist is free may be insufficient to guarantee that the position of the biopsy target T is fixed, a second controller is proposed that uses brakes and simultaneously emulates a spring behavior for Point P. Note that, as long as the brakes are ON and do not slip, bodies 3, 4, 5, and 6 of the robot constitute a same solid body. The velocity transmission model is obtained from (2) when considering that the three last joint velocities are null, which writes

$$\begin{pmatrix} \mathbf{v}_{6/0}(P) \\ \omega_{6/0} \end{pmatrix} = \begin{pmatrix} \mathbf{J}_{v1,P} \\ \mathbf{J}_{\omega 1} \end{pmatrix} \begin{pmatrix} \dot{\theta}_1 \\ \dot{\theta}_2 \\ \dot{\theta}_3 \end{pmatrix}. \tag{11}$$

Reciprocally, both a force and a moment can be applied to the probe at Point P, but only three actuators are controlled. The mapping from an external wrench applied to the probe to the three active joints torques is obtained by the dual of Eq. (11):

$$\begin{pmatrix} \tau_1 & \tau_2 & \tau_3 \end{pmatrix}^T = \mathbf{J}^T_{v1,P}\ \mathbf{f}_{6\to\mathrm{ext}} + \mathbf{J}^T_{\omega 1}\ \mathbf{m}_{6\to\mathrm{ext}}(P). \tag{12}$$

This last equation is to be understood as follows: with three actuators only, one cannot control both a force and a moment at Point P. However, for any wrench $(\mathbf{f}_{6\to\mathrm{ext}}, \mathbf{m}_{6\to\mathrm{ext}}(P))$, Eq. (12) can be used to computed a set of three joint torques that are *equivalent* to this wrench. In other words, they will produce the same mechanical effect on the system constituted by the end-effector probe and the three robot links.

For these reasons, although with the brakes on the gravity wrench now consists of six nonnull components at Point P, it can be compensated for thanks to a combination of (12) and (5)

$$\tau_{g,b} = -m\left(\mathbf{J}^T_{v1,P}\mathbf{g} + \mathbf{J}^T_{\omega 1}\left(\mathbf{g} \times \mathbf{d}_{GP}\right)\right). \tag{13}$$

The second controller uses this new gravity compensation term in addition to the spring emulation at Point P

$$\tau_{\mathrm{LMC-B}} = \tau_{g,b} + \tau_{k,P} \tag{14}$$

where $\tau_{k,P}$ is defined in Eq. (8). Here again, in order to guarantee a good static precision for the positionning of Point P, an external integrator is added, which leads to the controller depicted in Fig. 9. The same gain $\lambda = 4\ \mathrm{s}^{-1}$ is used for the external integrator.

3) Third Controller: Although brakes are used with the LMC-B controller, and although the external integrator ensures a null steady state error at Point P, the system may suffer from a lack of positioning precision at Point T. Indeed, the stiffness of the wrist brakes is not infinite and the probe orientation around Point P may be affected by external forces between the probe and the rectum. For this reason, it may be desirable to control the position of Point T instead of Point P, with the brakes on.

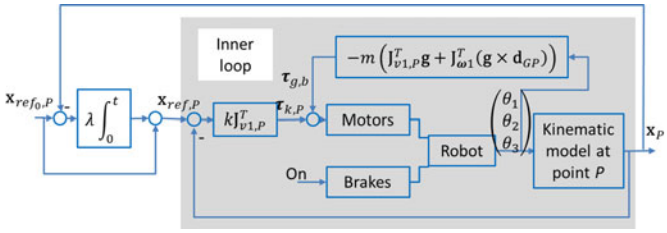

Fig. 9. Second control scheme in the locked mode (LMC-B).

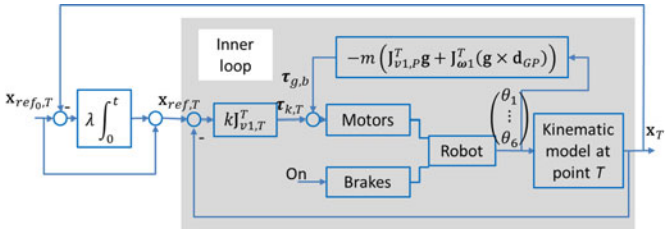

Fig. 10. Third control scheme in the locked mode (LMC-C).

This leads to the third controller, called LMC-C

$$\tau_{\mathrm{LMC-C}} = \tau_{g,b} + \tau_{k,T} \tag{15}$$

where $\tau_{g,b}$ is defined in Eq. (13) and

$$\tau_{k,T} = \mathbf{J}_{v1,T}^{T} k \left(\mathbf{x}_{\mathrm{ref},T} - \mathbf{x}_{T}\right). \tag{16}$$

In this last equation, k is a stiffness coefficient, $\mathbf{x}_T$ (resp. $\mathbf{x}_{\mathrm{ref},T}$) is the actual (respectively desired) position of Point T in the fixed frame $\mathscr{F}_0$, which can straightforwardly be computed from $\mathbf{q}$ though the robot's direct kinematics model and $\mathbf{J}_{v1,T}$ is the 3×3 subJacobian matrix that maps the velocity of the three active joints to the velocity of Point T

$$\mathbf{v}_{6/0}(T) = \mathbf{J}_{v1,T} \begin{pmatrix} \dot{\theta}_1 \\ \dot{\theta}_2 \\ \dot{\theta}_3 \end{pmatrix}. \tag{17}$$

In other words, $\tau_{k,T}$ in Eq. (16) corresponds a torque *equivalent* to a wrench composed of a null moment at Point T and a force proportional to the positioning error of Point T.

Here again, the spring behavior at Point T may lead to position errors in the presence of external disturbances. To cope with this problem, an external integrator for the position of Point T is added

$$\mathbf{x}_{\mathrm{ref},T} = \mathbf{x}_{\mathrm{ref}_0,T} + \lambda \int_0^t \left(\mathbf{x}_{\mathrm{ref}_0,T} - \mathbf{x}_T(u)\right) du \tag{18}$$

where $\mathbf{x}_{\mathrm{ref}_0,T}$ is the position of Point T recorded when the locked mode is switched on. In practice, λ is set to $0.4\mathrm{s}^{-1}$. The resulting control scheme is depicted in Fig. 10.

To summarize, Fig. 11 shows the mechanical equivalents of the three controllers, where the arrows show the movement produced at the reference point of the inner loop thanks to the integral outer loop. Clearly, LMC-C is expected to bring a better precision at Point T, our aim here was to evaluate whether this improvement is worth the cost of brakes and sensors to equip the wrist.

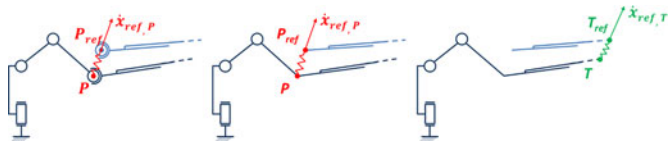

Fig. 11. Equivalent mechanical behavior for the three proposed controllers (from left to right, LMC-A to LMC-C).

B. *In-vitro Experiments*

In this section, Apollo's ability to maintain the probe at a given location, in the locked mode, is evaluated.

In the clinical scenario, the robot being initially in the free mode, the urologist manipulates the probe and places it at a desired location (e.g., to align the needle-guide attached to the probe with the biopsy target). Once satisfied with the probe position, he/she sets the locked mode on and releases the probe. Because the force disturbance arising from the probe-rectum contact is unknown and since the robot is given a low stiffness, unavoidably, the probe moves when released. Our aim here is to quantify this displacement and to verify Apollo's ability to compensate for it. This corresponds to the ability of the position control loop to reject the external force disturbance. It depends on the magnitude of the force disturbance and its direction, but not on the users experience. For this reason, an experiment was conducted with one urologist only.

In order to reproduce the variety of disturbances experienced in the clinical context, the urologist was asked to comanipulate the probe inserted in a prostate phantom (model 053, manufactured by CIRS). This phantom replicates both the anatomical biomechanics (similar amount of stiffness and friction) and the echogenicity of the prostate. During the experiments, the urologist had to position the probe at twelve different locations, according to the sextant scheme used in the clinical practice (see Fig. 12, upper left).

In order to monitor the adequate positioning of the probe, the urologist was using a Urostation, produced by the company Koelis (La Tronche, France). This system, which is approved for clinical use, is connected to a 3-D ultrasound machine (Samsung Medison accuvix V20) and includes an algorithm that accurately registers two 3-D ultrasound images of a prostate even in the presence of significant deformations. The protocol used for these experiments is similar to the clinical protocol. First, immediately after introducing the probe in the patient's rectum (here: the phantom), the urologist records a reference 3-D US image. This image is displayed on a screen interface. Then the urologist moves the probe towards a desired location, following the sextant scheme. To this aim, he uses the real time 2-D US image and mental reconstruction of the anatomical geometry. When he thinks he has reached the adequate location, he records a new 3-D US image which is registered to the reference 3-D image by the Urostation. Knowing the displacement computed by the registration algorithm, the Urostation displays, in the initial reference 3-D US image, the expected location of the biopsy needle, represented with a thin cylinder, as illustrated in Fig. 12–up-right. The urologist can then adapt the probe position until he has reached a position he estimates to be satisfactory.

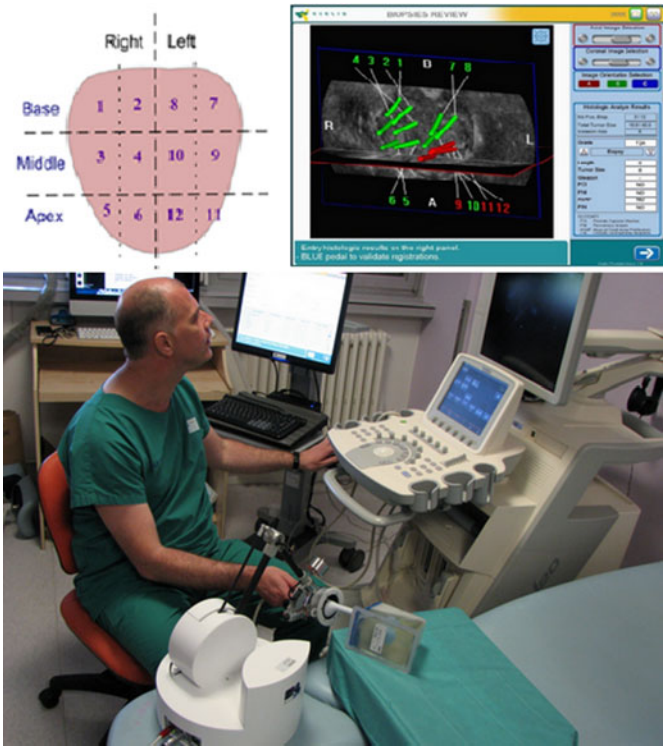

Fig. 12. Upper left: the sextant scheme used to position the probe during the *in-vitro* experiments. Upper right: a typical image from Urostation, allowing the urologist to visualize the location of a biopsy in a prostate. Bottom: setup with the phantom and the robot.

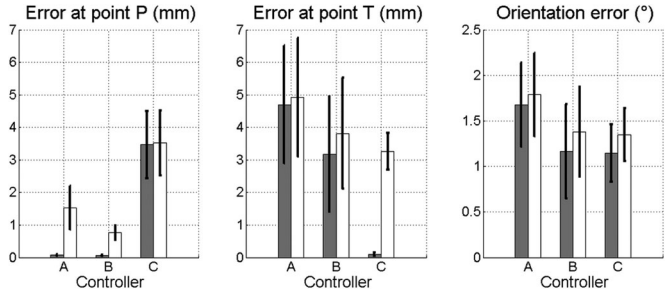

Fig. 13. Maximal and steady-state errors for each considered control laws (gray: steady state error; white: maximal error; black bars: standard deviation among the corresponding measurements).

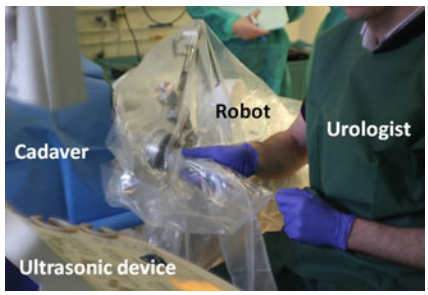

Fig. 14. *In-cadavero* experiments.

At this time, he selects the locked mode for the robot. The joint robot positions are recorded to set the reference for the external integrators.

C. Results

When the urologist locks the device and releases the probe handle, the typical behavior is as follows: in a first phase, the probe moves due to the wrench applied by the probe on the prostate phantom. Within a few seconds, thanks to the slow integration of the external loop, the system reaches its steady state, when the error controlled by the integrator has been canceled out.

To quantitatively analyze this behavior, for each experiment, Point P position error ($\|\mathbf{x}_{\mathrm{ref}_0,P} - \mathbf{x}_P\|$), Point T position error ($\|\mathbf{x}_{\mathrm{ref}_0,T} - \mathbf{x}_T\|$), and orientation error (defined as the positive geodesic distance between the probe orientation recorded when the locked mode is switched on and the current probe orientation) are computed. Fig. 4(c) shows the maximal and steady state values for these three positive errors, for each of the three control modes, averaged across the 12 sextant positions. In the left column, it can be observed that, as expected, the steady state error is null for Point P with LMC-A and LMC-B, due to the explicit integration of Point P position error. However, due to orientation errors (right column), Point T position is not precisely controlled and its positioning error reaches, in average, 4.7 mm with LMC-A and 3.1 mm with LMC-B. The effect of the brakes is visible on the right column, were the orientation errors are displayed. The brakes allow to limit the steady-state orientation error to 1.2° in average (for LMC-B and LMC-C), while it reaches 1.7° in average when the wrist is free of moving for LMC-A. The increase of precision for Point T position between LMC-A and LMC-B (middle column) is a direct consequence of the improvement in orientation control. Point T position is precisely controlled only with LMC-C (middle column) due to the integrator that cancels out its positioning error.

Clearly, with the selected low impedance for the inner stiffness loop, steady-state errors observed for Point T with LMC-A and LMC-B prevent for transfer to clinical applications. Indeed, an error bigger than 2–3 mm is too important when compared to the size of a clinically significant tumor [26]. This precision is to be measured at point T, which is the location of the biopsy, and not at point P. Therefore, the LMC-C mode will be kept in the further developments toward clinical transfer. Moreover; it shall be noticed that, from a clinical point of view, the 1.5° precision for the orientation is largely sufficient. Indeed, the biopsy location is mostly considered, from a clinical point of view, as a 3-D point, there is no clinical specification for the orientation, which is determined by the anatomical constraints imposed by the patients rectal anatomy. In conclusion, Apollo, equipped with brakes and position sensors for the wrist, and exploiting the controller LMC-C, is able of precisely locking the probe: when the urologist has manually placed the probe to point towards a desired 3-D biopsy location (point T) and then released the probe, Apollo automatically compensated for the probe weight and for any other disturbances, maintaining the point T still with a high precision. Only an orientation error persists, which has no importance from a clinical point of view.

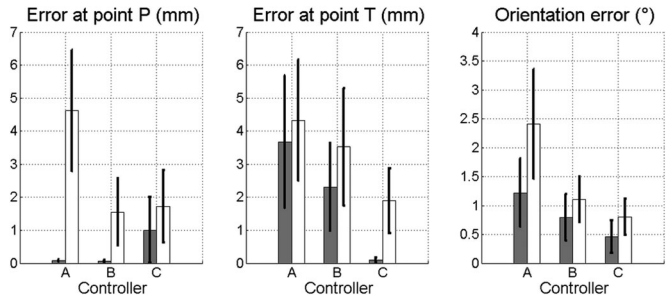

Fig. 15. Maximal and steady-state errors for each considered control laws (gray: steady state error; white: maximal error; black bars: standard deviation among the corresponding measurements).

V. *In-Cadavero* Experiments

Experiments have been conducted *in cadavero* at the Surgical School of Assistance Publique—Hopitaux de Paris. Two sessions were organized, each of them involving a fresh cadaver. Two urologists (a novice and an expert) were comanipulating the system during each of the two sessions.

A first aim was to verify the geometry. The two urologists were asked to scan the whole prostate with the probe using the ultrasound image, as they would do during a conventional examination. It appeared that the robot workspace was satisfying, whether the cadaver was in left lateral decubitus or in lithotomy position, lying down with feet in stirrups. No fastidious setup was required for any of the two body positions: the robot was simply positioned on the table or on a stool, without precise prepositioning. The first try for placing the robot base was satisfactory and convenient to perform all the experiments in both suject positions and for both subjects. Moreover, the urologists declared they felt comfortable and not disturbed in their gesture by the robot in free mode.

Locking experiments were then performed to evaluate the three proposed controllers for the locked mode. As compared to the *in-vitro* experiments, there were three differences in the setup.

1) Instead of using a phantom, the probe was inserted in a cadaver rectum;
2) The prostate could not be properly imaged due to the tissue deterioration, thus the Urostation was not used. Instead, the urologists targeted the biopsy sites based on their sole experience, without navigation or localization assistance, in accordance with the current clinical practice.
3) The ultrasound machine model was Sonix RP, manufactured by Ultrasonix.

Results are presented in Fig. 15. They are perfectly consistent with the *in-vitro* experiments.

VI. Conclusion

In this paper, we presented the design of a comanipulator for assisting endorectal prostate biopsies. This lightweight system, based on conventional robotic components, possesses 6 DoF but uses only three electric motors and three basic brakes. It features a free mode, where its low friction and inertia allows for natural manipulation of the probe and a locked mode, exhibiting both a very low stiffness and a high steady state precision.

A step toward clinical application was made thanks to *in-cadavero* experiments, as the robot appeared to bring significant help in the locked mode while not disturbing the urologist in the free mode.

One of the goals of this study was to determine the minimal equipment required for precisely maintaining the biopsy target immobile in the locked mode. Both *in-vitro* and *in-cadavero* experiments indicate that large errors may occur due to external forces when the wrist is not equipped with brakes and joint sensors. Brakes and joint sensors mounted on the wrist allow, with the adequate control law, to precisely maintain the biopsy target location with only three motors. They will, thus, be kept for the development of an industrial prototype targeting a clinical application. Meanwhile, one future development will consider working on expressing the control reference in the ultrasound image frame (visual servoing), in order to improve the effective precision.

References

[1] American Cancer Society. [Online]. Available: http://www.cancer.org
[2] P. Stattin, E. Holmberg, J.-E. Johansson, L. Holmberg, J. Adolfsson, J. Hugosson, and on behalf of the National Prostate Cancer Register (NPCR) of Sweden, "Outcomes in localized prostate cancer: National prostate cancer register of sweden follow-up study," *J. Nat. Cancer Inst.*, vol. 102, no. 13, pp. 950–958, 2010.
[3] G. Lu-Yao, P. Albertsen, D. Moore, W. Shih, Y. Lin, R. S. DiPaola, M. J. Barry, A. Zietman, M. O'Leary, E. Walker-Corkery, and S. L. Yao, "Outcomes of localized prostate cancer following conservative management," *JAMA*, vol. 302, no. 11, pp. 1202–1209, 2009.
[4] N. N. Stone, J. Roy, S. Hong, Y.-C. Lo, and R. G. Stock, "Prostate gland motion and deformation caused by needle placement during brachytherapy," *Brachytherapy*, vol. 1, no. 3, pp. 154–160, 2002.
[5] V. Lagerburg, M. A. Moerland, J. J. Lagendijk, and J. J. Battermann, "Measurement of prostate rotation during insertion of needles for brachytherapy," *Radiotherapy Oncol.*, vol. 77, no. 3, pp. 318–323, 2005.
[6] N. Hungr, M. Baumann, J. Long, and J. Troccaz, "A 3-d ultrasound robotic prostate brachytherapy system with prostate motion tracking," *IEEE Trans. Robot.*, vol. 28, no. 6, pp. 1382–1397, Dec. 2012.
[7] S. Salcudean, T. Prananta, W. Morris, and I. Spadinger, "A robotic needle guide for prostate brachytherapy," in *Proc. IEEE Int. Conf. Robot. Autom.*, May 2008, pp. 2975–2981.
[8] H. Ho, P. Mohan, E. Lim, D. Li, J. Yuen, W. Ng, W. Lau, and C. Cheng, "Robotic ultrasound-guided prostate intervention device: system description and results from phantom studies," *Int. J. Med. Robot. Comput. Assisted Surg.*, vol. 5, no. 1, pp. 51–58, 2009.
[9] G. Fischer, I. Iordachita, C. Csoma, J. Tokuda, S. DiMaio, C. Tempany, N. Hata, and G. Fichtinger, "Mri-compatible pneumatic robot for transperineal prostate needle placement," *IEEE/ASME Trans. Mechatronics*, vol. 13, no. 3, pp. 295–305, Jun. 2008.
[10] A. Patriciu, D. Petrisor, M. Muntener, D. Mazilu, M. Schar, and D. Stoianovici, "Automatic brachytherapy seed placement under MRI guidance," *IEEE Trans. Biomed. Eng.*, vol. 54, no. 8, pp. 1499–1506, Aug. 2007.
[11] S.-E. Song, N. Cho, G. Fischer, N. Hata, C. Tempany, G. Fichtinger, and I. Iordachita, "Development of a pneumatic robot for mri-guided transperineal prostate biopsy and brachytherapy: New approaches," in *Proc. IEEE Int. Conf. Robot. Autom.*, May 2010, pp. 2580–2585.
[12] G. Fichtinger, T. L. DeWeese, A. Patriciu, A. Tanacs, D. Mazilu, J. H. Anderson, K. Masamune, R. H. Taylor, and D. Stoianovici, "System for robotically assisted prostate biopsy and therapy with intraoperative CT guidance," *Academic Radiol.*, vol. 9, no. 1, pp. 60–74, 2002.
[13] L. Phee, D. Xiao, J. Yuen, C. F. Chan, H. Ho, H. Choon, C. Christopher, and S. N. Wan, "Ultrasound guided robotic system for transperineal biopsy of the prostate," in *Proc. IEEE Int. Conf. Robot. Autom.*, Apr. 2005, pp. 1315–1320.

[14] Z. Wei, M. Ding, D. Downey, and A. Fenster, "3d trus guided robot assisted prostate brachytherapy," in *Medical Image Computing and Computer-Assisted Intervention MICCAI 2005*, (Lecture Notes in Computer Science Series), J. Duncan and G. Gerig, Eds., Berlin, Germany: Springer, vol. 3750, pp. 17–24, 2005.
[15] H. Bassan, T. Hayes, R. Patel, and M. Moallem, "A novel manipulator for 3d ultrasound guided percutaneous needle insertion," in *Proc. IEEE Int. Conf. Robot. Autom.*, Apr. 2007, pp. 617–622.
[16] G. Fichtinger, J. P. Fiene, C. W. Kennedy, G. Kronreif, I. Iordachita, D. Y. Song, E. C. Burdette, and P. Kazanzides, "Robotic assistance for ultrasound-guided prostate brachytherapy," *Med. Image Anal.*, vol. 12, no. 5, pp. 535–545, 2008.
[17] T. Podder, W. S. Ng, and Y. Yu, "Multi-channel robotic system for prostate brachytherapy," in *Proc. 29th Annu. Int. Conf. Eng. Med. Biol. Soc.*, Aug. 2007, pp. 1233–1236.
[18] M. R. van den Bosch, M. R. Moman, M. van Vulpen, J. J. Battermann, E. Duiveman, L. J. van Schelven, H. de Leeuw, J. J. W. Lagendijk, and M. A. Moerland, "MRI-guided robotic system for transperineal prostate interventions: proof of principle," *Phys. Med. Biol.*, vol. 55, no. 5, p. N133, 2010.
[19] C. Schneider, A. Okamura, and G. Fichtinger, "A robotic system for transrectal needle insertion into the prostate with integrated ultrasound," in *Proc. IEEE Int. Conf. Robot. Autom.*, Apr./May 2004, vol. 1, pp. 365–370.
[20] A. Krieger, I. Iordachita, P. Guion, A. Singh, A. Kaushal, C. Menard, P. Pinto, K. Camphausen, G. Fichtinger, and L. Whitcomb, "An MRI-compatible robotic system with hybrid tracking for mri-guided prostate intervention," *IEEE Trans. Biomed. Eng.*, vol. 58, no. 11, pp. 3049–3060, Nov. 2011.
[21] C. Torterotot, P. Mozer, M. Baumann, M. Vitrani, and G. Morel, "Analysis of endorectal probe kinematics during prostate biopsies," in *Proc. Hamlyn Symp. Med. Robot.*, 2010, pp. 47–48.
[22] J. Denavit and R. S. Hartenberg, "A kinematic notation for lower-pair mechanisms based on matrices," *Trans. ASME, J. Appl. Mech.*, vol. 23, pp. 215–221, 1955.
[23] Haption. [Online]. Available: http://www.haption.fr
[24] N. Jarrasse, J. Paik, V. Pasqui, and G. Morel, "How can human motion prediction increase transparency?," in *Proc. IEEE Int. Conf. Robot. Autom.*, Pasadena, CA, USA, May. 2008, pp. 2134–2139.
[25] S. Balasubramanian, A. Melendez-Calderon, and E. Burdet, "A robust and sensitive metric for quantifying movement smoothness," *IEEE Trans. Biomed. Eng.*, vol. 59, no. 8, pp. 2126–2136, Aug. 2012.
[26] M. Terris, J. McNeal, and T. Stamey, "Detection of clinically significant prostate cancer by transrectal ultrasound-guided systematic biopsies," *J. Urology*, vol. 148, no. 3, pp. 829–832, 1992.

Cécile Poquet studied at the Ecole Normale Suprieure de Cachan, Cachan, France, one of the French Grandes Ecoles dedicated to higher education and research, from 2006 to 2010. She received the M.S. degree in advanced and robotic systems in 2010 from the University Pierre and Marie Curie, Paris, France, where she has been working toward the Ph.D. degree since September 2010.

She is currently working on the assistance to prostate biopsies through comanipulation at the Institute of Intelligent Systems and Robotics, Paris.

Pierre Mozer received the M.D. degree from the University of Paris VI, Paris, France, in 2002, and the Ph.D. degree from Grenoble University, Grenoble, France, in 2007.

He has been an Assistant Professor in the Department of Urology, Groupe Hospitalier Piti-Salptrire, Paris. He also holds a postdoctoral position in the Institute of Intelligent Systems and Robotics Laboratory, Paris. His research interests include computer-aided surgery in all fields of urology, in particular, for kidney, prostate, and incontinence.

Marie-Aude Vitrani received the Ph.D. degree in robotics from the University Pierre and Marie Curie (UPMC), Paris, France, in 2006.

Since 2007, she has been an Assistant Professor of mechanical engineering at UPMC. Her research interests include the design and control of robotic systems for assistance to medical gestures, with a particular focus on ultrasound-image-based guidance and ultrasound probe placement.

Guillaume Morel received the Ph.D. degree in control engineering from the University of Paris 6, Paris, France, in 1994.

From 1995 to 1996, he was a Postdoctoral Research Assistant at the Massachusetts Institute of Technology, Cambridge, MA, USA, and, from 1997 to 2001, an Assistant Professor at the University of Strasbourg, Strasbourg, France. He was an Assistant Professor of mechanical engineering at the University of Pierre and Marie Curie—Paris 6, Paris, from 2001 to 2006, where he is currently a Professor of robotics and leads the research team AGATHE (INSERM U1150) within the Institute of Intelligent Systems and Robotics (UMR UPMC–CNRS 7222). His research interests include sensor-based control of robots, with a particular focus on force feedback control and visual servoing. His research targets applications to assistance for surgery and rehabilitation systems.